Available online at www.sciencedirect.com
SCIENCE DIRECT®
ELSEVIER
European Journal of Mechanics B/Fluids 23 (2004) 737–758
EUROPEAN JOURNAL OF MECHANICS B/FLUIDS

Analysis of a stochastic backscatter model for the large-eddy simulation of wall-bounded flow

P.S. Westbury [a], D.C. Dunn [a,b], J.F. Morrison [a,*]

[a] *Department of Aeronautics, Imperial College, London SW7 2AZ, UK*
[b] *School of Mathematics, University of Bristol, University Walk, Bristol BS8 1TW, UK*

Available online 9 April 2004

Abstract

The stochastic backscatter model of Mason and Thomson (1992) has been analysed using direct numerical simulation databases of turbulent channel flow at $Re_\delta = 300$. Backscatter is quantified using a number of different filters with cutoffs at wavenumbers corresponding to an inertial subrange at high Reynolds numbers. Since the model finds greatest application at meteorological Reynolds numbers, the implications of using low-Reynolds-number data are addressed. Probability distributions of the energy transfer obtained both directly from the DNS data and using the stochastic model are compared by matching the first moments and using a single tuneable constant to optimise agreement of the variances. It is found that the probability distributions essentially have the same shape, illustrating the model's ability to represent the backscatter correctly outside the viscous sublayer. However, the model consistently underestimates the non-Gaussian behaviour of the energy transfer and some suggestions have been made to remedy this. Probability distributions of the energy transfer conditional on the square of the resolved strain rate show that a range of values of transfer exist for one value of strain rate.

Keywords: Stochastic backscatter; Large-eddy simulation; Wall turbulence

1. Introduction

Large-eddy simulation (LES) of turbulent flow involves the explicit calculation of the large-scale, resolved motions using the spatially filtered Navier–Stokes equations. The energy transfer between the resolved scales and unresolved, "subgrid" scales is modelled. General reviews are provided by Spalart [1] and Jiménez and Moser [2]. The well-founded premise of LES is that turbulence exhibits a greater degree of universality in the small scales compared with the turbulence field taken as a whole, and therefore a successful closure, with a wider range of application, is more likely to be achieved by LES than by closures of the Reynolds-averaged equations. However, a particular difficulty in LES is how best to model the net drain of energy from the resolved scales to the subgrid scales. Many workers [3–8] have shown that, in fact, the transfer is bi-directional and that non-linear interactions between the resolved scales and the subgrid scales cause both "forward scatter" (positive transfer out of the resolved scales) as well as "backscatter", the reverse transfer of energy from the subgrid to the resolved scales.

Most traditional subgrid modelling is based on the Smagorinsky model [9] which employs a simple eddy viscosity to relate the resolved-scale strain rate to the subgrid stresses. Simulation of the interior flow is relatively insensitive to the choice of subgrid model (Bardina et al. [10], Mason and Brown [11]), since, away from a surface, most of the energy-containing eddies are resolved and the details of the subgrid motions have little effect. Thus the theoretical basis for large-eddy simulation is reasonably well-founded because the division of the resolved and subgrid scales can occur in an inertial subrange, resulting

* Corresponding author.
E-mail address: j.morrison@imperial.ac.uk (J.F. Morrison).

0997-7546/$ – see front matter
doi:10.1016/j.euromechflu.2004.01.003

in a clear distinction between the energy-producing and energy-dissipating scales; ideally, the production should be effected entirely by the resolved scales and the dissipation by the subgrid scales. In the case of implicit filtering, Muschinski [12] uses Kolmogorov's theory to define suitable values for the Smagorinsky coefficient and to illustrate how its value determines the relationship between the filter length scale and the mesh size.

However, such models are unable to represent the complicated energy-transfer processes occurring near surfaces, where all the eddies are 'small' and where backscatter predominates [13], because, invariably, they use the concept of an eddy viscosity which is, by definition, absolutely dissipative. A negative value of eddy viscosity can lead to numerical instability. Forward scatter and backscatter are defined by the filter – they are not necessarily the same as the spectral flux of energy in Fourier space across a given wavenumber. Evidence for the existence of backscatter is provided by the theoretical work of Leslie and Quarini [14], who suggest that backscatter should be modelled separately from the energy drain. In particular they show that the backscatter rate in the inertial subrange scales with the mean turbulence dissipation rate, ε. A number of workers [15,16] have developed subgrid models which are able to represent backscatter. In particular, Mason and Thomson [15], Leith [17] and Schumann [18] have used the Smagorinsky model as the basis for their subgrid models, but have added random stress fluctuations which give rise to stochastic backscatter.

The advent of accurate direct numerical simulation (DNS) databases has made possible numerous studies on the detailed nature of the subgrid stresses and energy transfers [5,3,19]: these studies show that, in the viscous sublayer, regions of forward scatter and backscatter are correlated with the appearance of coherent structures which occur intermittently in time and space. Meneveau [8] has used a wavelet decomposition of the fluctuating part of the velocity field to identify regions of large energy transfer in sheared homogeneous turbulence. Dunn and Morrison [20–23] have used similar algorithms to investigate the role of structure in the anisotropy of energy transfer, nearly all of which involves subgrid flux of streamwise momentum in the wall-normal and spanwise directions. They also show that, consistent with nearly all current subgrid models, the pressure-gradient term effects negligible energy transfer. Akhavan et al. [24] have shown that spectral energy transfer arises through local as well as non-local interactions. The non-local interactions lead to forward scatter and therefore are suitably modelled by an eddy viscosity. However, the local transfers are bi-directional and arise through the presence of organised vortical structures. This suggests that they are unlikely to be modelled successfully by a stochastic force. Dunn and Morrison [22] find a similar divison between non-local and local transfers in wall turbulence. Using the dynamic subgrid model, Carati et al. [25] have made a detailed assessment of stochastic and deterministic models of backscatter in isotropic decaying and forced turbulence: they suggest that the way in which backscatter is accounted for does not appear to play a major role in the simulations. Experimental data, which are not restricted to the low Reynolds numbers of DNS data, have also been used to analyse the subgrid stresses and to evaluate the performance of subgrid models [26,27]. Meneveau [28] has suggested that the low-order statistics of the energy transfer are a sufficent condition for a subgrid model to be considered sound.

In high-Reynolds-number LES of wall-bounded flows, it is important to use an "off-the-surface" boundary condition in order to avoid resolution of the viscous wall region [29]. For the lack of an alternative, many workers have used the logarithmic law despite the fact that it does not apply to the time-resolved flow field [30]. Moreover, in the vicinity of the matching region (that between the surface and the lowest mesh point), the bi-directional transfer of energy between the resolved motion and the subgrid scales will be large. Therefore a subgrid model with a stronger physical basis than that provided by the Smagorinsky model is required. Mason and Thomson [15] have shown that the Smagorinsky model is unable to reproduce the correct logarithmic mean velocity profile near the surface, but with the inclusion of a stochastic backscatter model, a notable improvement to the agreement between the mean velocity profile and the log law is obtained. The subgrid stress fluctuations are scaled to give the correct backscatter rate, estimated using physical and dimensional reasoning. While EDQNM theory [31] provides an estimate of the backscatter in the flow interior, there is no theoretical basis for estimating the magnitude and detail of the backscatter in the near-surface region [13]. The actual model constants were therefore tuned to provide agreement with the log law.

The purpose of the present work is to carry out a quantitative analysis of the energy transfer between the resolved and the subgrid scales, using DNS data of turbulent channel flow, and so quantify the magnitude of the backscatter. In particular, the DNS data are used to assess the Mason and Thomson stochastic backscatter model [15]. By filtering the DNS data, the nature of the interaction between the resolved and subgrid scales can be investigated. The quantities which are available from the resolved scales of a large-eddy simulation can also be calculated, and these are necessary for determining the energy transfer predicted by the model. Analysis of the DNS data yields probability distributions of the energy transfer rate between the resolved and subgrid scales, which can be compared to the probability distributions obtained from the Mason and Thomson model. In order to account for the low Reynolds number of the DNS data, they are analysed so that production in the subgrid scales and direct viscous dissipation in the resolved scales are separated out [3]. The principle concern to be addressed is whether or not stochastic forcing provides a reliable model of backscatter in near-wall turbulence [24,25].

In the following section, the equations for large-eddy simulation are given. Section 3 presents the methodology for testing the Mason and Thomson stochastic backscatter model. A brief description of the databases is provided in Section 4. The choice of filters used in the analysis is discussed in Section 5, and in Section 6, consideration is given to the effects of using DNS data

at low Reynolds number. Section 7 compares results of the analysis of energy transfers, obtained directly from the DNS data with those from the stochastic backscatter model.

2. LES equations

The equations for the evolution of the resolved scales is obtained by filtering the Navier–Stokes equations:

$$\frac{\partial \tilde{u}_i}{\partial t} + \frac{\partial \tilde{u}_i \tilde{u}_j}{\partial x_j} = -\frac{1}{\rho}\frac{\partial \tilde{p}}{\partial x_i} - \frac{\partial \tau_{ij}}{\partial x_j} + \nu \frac{\partial^2 \tilde{u}_i}{\partial x_j \partial x_j}; \tag{1}$$

and the filtered velocity field satisfies the continuity equation:

$$\frac{\partial \tilde{u}_i}{\partial x_i} = 0, \tag{2}$$

where tilde denotes a filtered quantity. The term which represents the effect of the subgrid scales on the large, resolved scales is the subgrid stress term:

$$\tau_{ij} = \widetilde{u_i u_j} - \tilde{u}_i \tilde{u}_j. \tag{3}$$

The energy transfer between resolved and subgrid scales is,

$$T = -\tau_{ij} \widetilde{S}_{ij}, \tag{4}$$

where $\widetilde{S}_{ij}$ is the large-scale strain rate:

$$\widetilde{S}_{ij} = \frac{1}{2}\left(\frac{\partial \tilde{u}_i}{\partial x_j} + \frac{\partial \tilde{u}_j}{\partial x_i} \right). \tag{5}$$

T is taken to be positive when the energy transfer is from large scales to small scales, and negative when there is a reverse transfer of energy. So that the subgrid stresses are trace-free as is the resolved strain-rate tensor, the isotropic part of the subgrid stress is usually removed and incorporated into the pressure term:

$$\tau_{ij}^{(I)} = \tau_{ij} - \frac{1}{3}\delta_{ij}\tau_{kk}. \tag{6}$$

However, for consistency with the backscatter model, the subgrid-scale stress is always calculated using Eq. (3). Finally, the subgrid-scale energy is given by:

$$\tau_{kk} = \widetilde{u_k u_k} - \tilde{u}_k \tilde{u}_k. \tag{7}$$

3. The stochastic backscatter model

The implementation of the stochastic backscatter model in the LES simulation is described in Mason and Thomson [15]. In order to facilitate comparison, a complete outline of the model is provided here. *A posteriori* testing of the model has already been performed by Mason and colleagues [11,13,15].

3.1. Energy transfer rate in the model

The random stress components used to model the backscatter are added into the time-stepping, leap-frog scheme, in which the random stresses are changed every second time-step. In the following analysis, the time scale for changes to the random stresses is Δt. Note that, in this section, the quantities S and u_i are the resolved quantities, where for clarity, tildes have not been used to denote them.

Expressed in finite-difference terms, the time-stepping scheme is given by:

$$u_i(t + \Delta t) = u_i(t) + f_i \Delta t + \frac{\partial \tau_{ij}}{\partial x_j}\Delta t, \tag{8}$$

where $f_i = \nabla \wedge \phi_i$ and ϕ_i is the vector potential generated using random numbers, and scaled to give the correct energy backscatter rate. The term $f_i \Delta t$ represents the backscatter. The definition of τ_{ij} is given by the usual Smagorinsky [9] model expression:

$$\tau_{ij} = \nu_{\mathrm{LES}}\left(\frac{\partial u_i}{\partial x_j} + \frac{\partial u_j}{\partial x_i} \right), \tag{9}$$

where ν_{LES}, the eddy viscosity, is given by:

$$\nu_{\mathrm{LES}} = l_s^2 S, \tag{10}$$

and

$$S^m = \left[\frac{1}{2}\left(\frac{\partial u_i}{\partial x_j} + \frac{\partial u_j}{\partial x_i}\right)^2\right]^{m/2}. \tag{11}$$

The Smagorinsky length scale, l, is usually, but not necessarily, related to the mesh size, Δ, by:

$$l = C_s \Delta, \tag{12}$$

where C_s is the Smagorinsky constant.

Squaring Eq. (8) and retaining only a single term $\mathrm{O}[(\Delta t)^2]$:

$$u_i u_i(t+\Delta t) = u_i u_i(t) + 2 f_i u_i \Delta t + 2 u_i \frac{\partial \tau_{ij}}{\partial x_j}\Delta t + f_i f_i \Delta t^2. \tag{13}$$

The Δt^2 term has been retained as part of the random forcing term, because without it, the backscatter does not, on average, cause a net input of energy. Thus:

$$u_i u_i(t+\Delta t) = u_i u_i(t) + \underbrace{2\nabla\cdot(\phi_i \wedge u_i)\Delta t}_{(1)} - \underbrace{2\phi_i\cdot(\nabla\wedge u_i)\Delta t}_{(2)} + \underbrace{2\frac{\partial}{\partial x_j}(u_i\tau_{ij})\Delta t}_{(3)} - \underbrace{2\nu_{\mathrm{LES}} S^2 \Delta t}_{(4)} + \underbrace{|f_i|^2\Delta t^2}_{(5)}. \tag{14}$$

The various terms are interpreted as follows: (1) the backscatter transport, which is separated out to ensure that the backscatter energy input is Galilean invariant; (2) the random part of the backscatter energy input, which averages to zero; (3) Smagorinsky transport; (4) Smagorinsky drain; (5) the systematic part of the backscatter energy, which has a non-zero average.

Thus the rate of energy input to the resolved scales is calculated using only terms (2), (4) and (5) is:

$$\text{rate of energy input} = -\phi_i\cdot(\nabla\wedge u_i) - \nu_{\mathrm{LES}} S^2 + |f_i|^2\Delta t \tag{15}$$

and $|f_i|^2$ is chosen to be of order $1/\Delta t$ so that the last term is O(1), while the first term on the right-hand side is much larger, but zero on average.

3.2. Probability distribution function (pdf) of modelled energy transfer

Following Leslie and Quarini [14], the model is designed so that:

$$\text{Mean backscatter rate} = C_B \times \varepsilon, \tag{16}$$

where ε is the mean (subgrid) dissipation rate and C_B is a constant. Thus the net backscatter rate is given by:

$$|f_i|^2\Delta t = C_B\left(\nu_{\mathrm{LES}} S^2 - |f_i|^2\Delta t\right) \tag{17}$$

and:

$$|f_i|^2\Delta t = \frac{C_B}{1+C_B}\nu_{\mathrm{LES}} S^2 = \frac{C_B}{1+C_B} l^2 S^3. \tag{18}$$

Eq. (18) represents the systematic backscatter. The random backscatter term is obtained by introducing L, the length scale of the ϕ variation. Then $\phi \sim (|f_i|^2)^{1/2} \times L$. Noting from Eq. (15) that the random backscatter term is $\phi_i\cdot(\nabla\wedge u_i)$, the *gross* energy transfer rate, T, is given by:

$$T = \frac{l^2 S^3}{1+C_B} + \left(\frac{C_B}{1+C_B}\frac{l^2 S^3}{\Delta t}\right)^{1/2} L\cdot(\nabla\wedge u_i) r, \tag{19}$$

where the first term on the right-hand side equals ε and the second term is the random backscatter rate. r is a Gaussian random number with mean $= 0$ and variance $= 1$. In the interior of the flow, l and L are likely to be the order of the filter scale, although nearer the surface, the situation is more complicated.

To make a meaningful comparison between the energy transfer predicted by the model and that calculated using the DNS data, it is assumed that the model is applied with Δt of order the subgrid turbulent time scale:

$$\Delta t \sim \frac{l^{2/3}}{\langle\varepsilon\rangle^{1/3}}, \tag{20}$$

where $\langle\varepsilon\rangle$ is the dissipation rate averaged over homogeneous planes of the DNS database. Allowing the backscatter term to operate bi-directionally:

$$T = \frac{l^2 S^3}{1+C_B} \pm \left(\frac{C_B}{1+C_B} \frac{l^2 S^3}{l^{2/3}} \langle\varepsilon\rangle^{1/3} \right)^{1/2} L|\nabla \wedge u_i| r. \tag{21}$$

Thus the modelled pdf of energy transfer, T, is estimated using:

$$T = \frac{l^2 S^3}{1+C_B} \pm a S^{3/2} \langle\varepsilon\rangle^{1/6} |\nabla \wedge u_i| l^{2/3} \left(\frac{C_B}{1+C_B} \right)^{1/2} l_f r, \tag{22}$$

where L is set to the filter scale, l_f and a is a tuneable constant. The value of l is adjusted so that the mean value of the model pdf is the same as that calculated using the DNS data. The tuneable constant, a (of order one), is introduced in order to account for numerical constants in $L \sim l_f,\ \Delta t \sim l^{2/3}/\langle\varepsilon\rangle^{1/3}$ and uncertainty in the value of C_B, which is taken as 1.4. a is varied to optimise agreement of the variances. Note that in Eq. (22), even though the random number, r, is Gaussian, $|\nabla \wedge u_i|$ is not. Therefore T is non-Gaussian also.

3.3. Treatment of near-surface effects

As the surface is approached, the main energy-containing eddies become smaller than the filter scale. In the implementation of the model the mixing length, l, is specified by the 'matching condition':

$$\frac{1}{l^2} = \frac{1}{l_0^2} + \frac{1}{(\kappa(z+z_0))^2}, \tag{23}$$

where κ is the von Kármán constant, and the exponent is adjusted to provide an optimum matching height. C_B is given by:

$$C_B = 1.4 \left(\frac{l}{l_0} \right)^5, \tag{24}$$

where l_0 is the mixing length in the flow interior, and $l_0 \propto l_f$. The exponent here derives from dimensional considerations of the model random stress fluctuations [15].

4. DNS databases

The analysis uses DNS databases as described by Sandham and Howard [32]: data are available for Reynolds number, Re_δ, based on wall friction velocity, u_τ, and channel half-height, δ, of 300. The domain is $13\delta \times 6\delta \times 2\delta$ in the x (streamwise), y (spanwise) and z (wall-normal) directions respectively. The number of grid points is $256 \times 256 \times 160$. The grid spacing in the streamwise direction is $\Delta x^+ \approx 15$ and in the spanwise direction is $\Delta y^+ \approx 7$. (Use of the superscript '+' with any variable denotes non-dimensionalsation with wall variables.) The grid-spacing in the wall-normal direction becomes finer nearer the wall due to Chebyschev-tau discretisation. The streamwise, spanwise and wall-normal velocity components are denoted, respectively, by $u_1 = u,\ u_2 = v$ and $u_3 = w$. Fig. 1(a) shows the u-component of the velocity spectra at three different values of z^+, non-dimensionalised using Kolmogorov's universal scaling:

$$\frac{E_{11}(k_1)}{(\varepsilon\nu^5)^{1/4}} = f(k^*), \tag{25}$$

where $k^* = k_1\eta,\ k_1$ is the wavenumber in the streamwise direction and η is the Kolmogorov length scale. Given that the existence of an inertial subrange is important in the context of LES, it is important to determine whether or not it appears at the Reynolds numbers of the DNS data. Values of Re_λ are 82.0, 65.7 and 43.2 at values of $z^+ = 68,\ 180$ and 294 respectively. Bradshaw [33] suggests $Re_\lambda \geqslant 100$ as a suitable criterion for the existence of a "first-order" inertial subrange, that is one in which it is required that the transfer at any wavenumber is much larger than sources or sinks: local isotropy is not a formal requirement. It is clear that only close to the wall does Re_λ approach this value. Note that a $-5/3$ slope is not a sufficient condition for the appearance of an inertial subrange [34,33,35]. Moreover, with Kolmogorov scaling, which also defines ε, collapse of the spectra on a universal spectrum provides an indication of the region in which a $-5/3$ slope (as distinct from an inertial subrange) can be expected. In Fig. 1(a), this region is given by $f(k^*) = C(k^*)^{-5/3}$, where $C \approx 0.49$. Fig. 1(b) shows energy spectra for the w-component of velocity, which shows rather different behaviour at low wavenumbers owing to the "impermeability constraint" which 'blocks' eddies at a distance from the wall that is roughly the inverse of the wavenumber. Therefore, this component offers a more rigorous test for the existence of a $-5/3$ region which extends over a slightly narrower

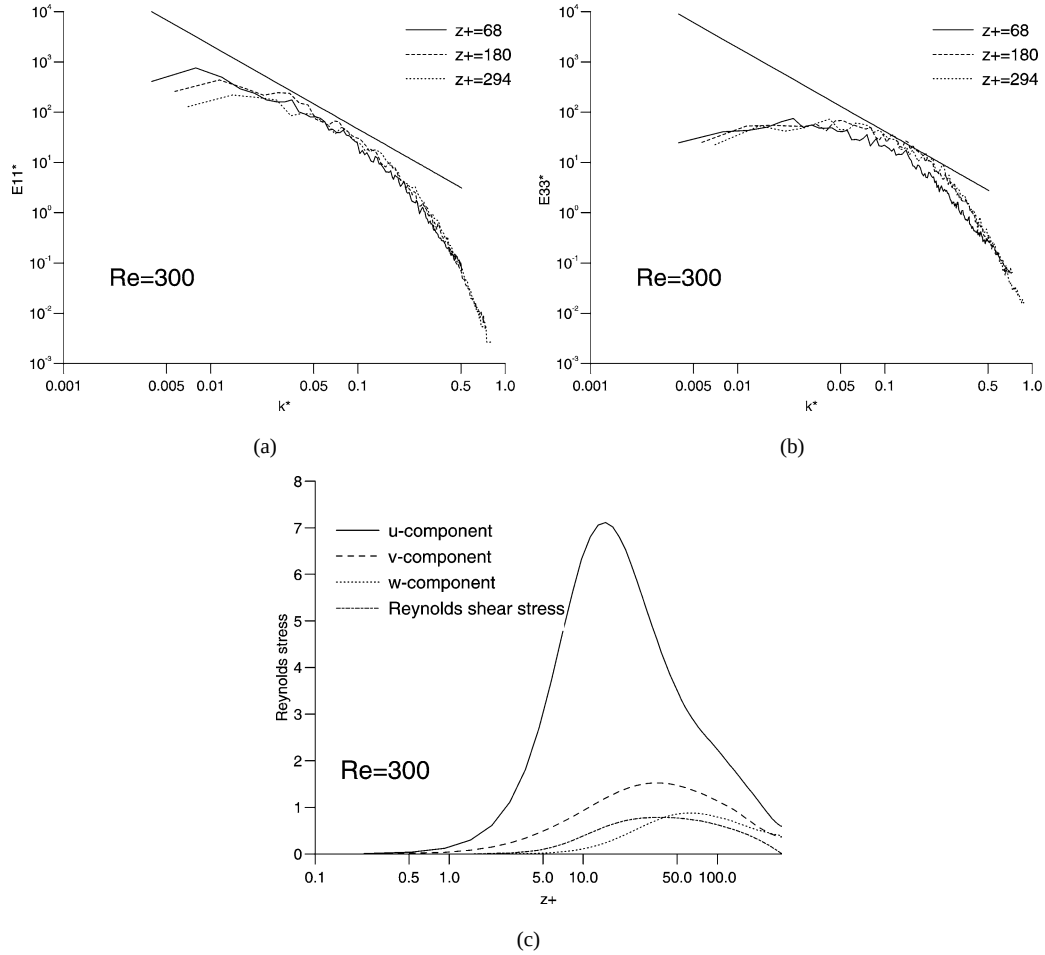

Fig. 1. Plots of (a) u-spectra; (b) w-spectra and (c) Reynolds stress profiles. Straight line has slope of $-5/3$ only; its values are not those of the inertial subrange.

range of k^* than that in Fig. 1(a). The estimates of Re_λ confirm that, near the lower limit of the logarithmic region, a $-5/3$ region can be expected. In Fig. 1(b), the inertial subrange constant is $\frac{4}{3} \times C$. These considerations are important in terms of the most appropriate choice of filter width. We address the issue of the suitability of low-Reynolds-number DNS data to the subgid model for high-Reynolds-number applications in Section 6.

5. Choice of filters

The LES algorithm of Mason and Thomson uses implicit filtering; therefore the Smagorinsky length scale, l_0, sets the scale of the filter (l_0 is theoretically related to a filter scale, l_f, by the expression $l_f = l_0/C_f$, where C_f is approximately equal to 0.2). Muschinski [12] shows how the value of C_s determines the relative influence of the mesh size and l_0 on the effective spatial filter, l_f. In the Mason and Thomson model, the shape of the effective filter is unclear. Muschinski also discusses the effective filter shape produced by implicit filtering of locally isotropic turbulence: he suggests that it is similar to a "diffuse cutoff of the inertial range TKE [turbulent kinetic energy] spectrum of Navier–Stokes turbulence at wavenumbers on the order of η^{-1}". For a comparison with the resolved scales in LES using a spectral method, Meneaveau [8] suggests that a Fourier cutoff filter should be applied to the DNS data, while a box filter should be employed if a finite-difference scheme is used. Furthermore, a Gaussian filter may produce resolved fields similar to those created by a large-eddy simulation which uses a "(hypothetical) wavelet method".

Owing to the uncertainty in the effective filter shape, the following filters are used with the DNS data: the Fourier cutoff filter,

$$\widehat{G}_i = \begin{cases} 1 & \text{if } k_i < K_i, \\ 0 & \text{otherwise;} \end{cases} \tag{26}$$

Table 1
Non-dimensional filter widths at $z^+ = 68$. Dimensional filter width does not vary with z^+

c	$K_1\eta$	$K_2\eta$	Δ_1^+	Δ_2^+
1	0.055	0.12	278	129
2	0.088	0.19	177	82
3	0.12	0.25	134	62

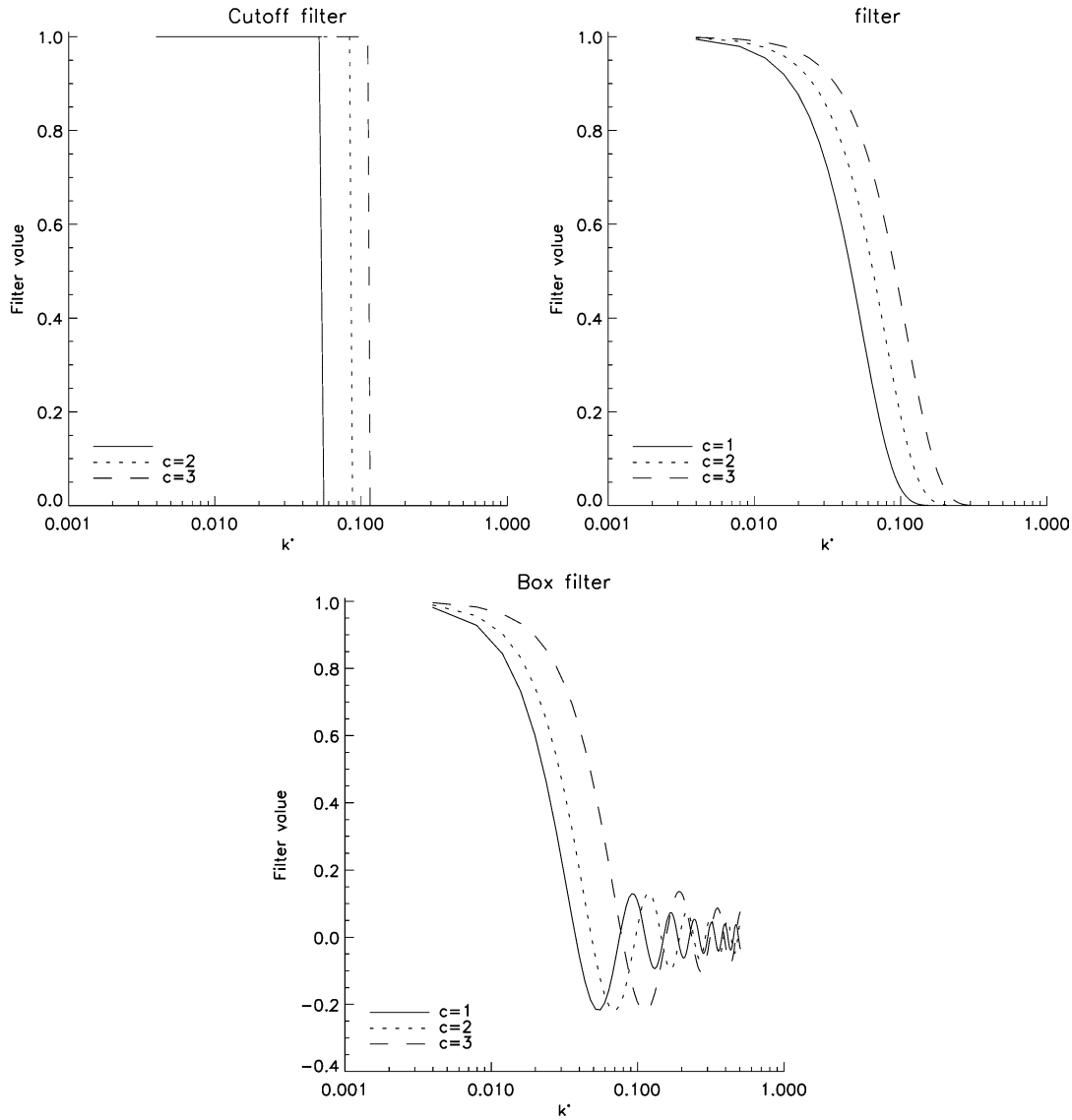

Fig. 2. Filter definitions for $z^+ = 68$.

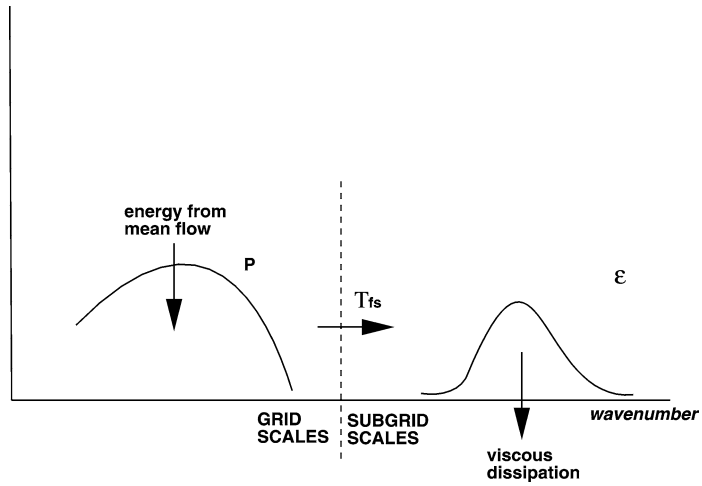

Fig. 3. LES modelling in high-Reynolds-number flow. Production, $\mathcal{P}$, and dissipation, ε, are well separated. The cutoff wavenumber lies in the inertial range and the effect of the subgrid-scale stresses is to drain the resolved scales at a rate $T^{FS} = \varepsilon$.

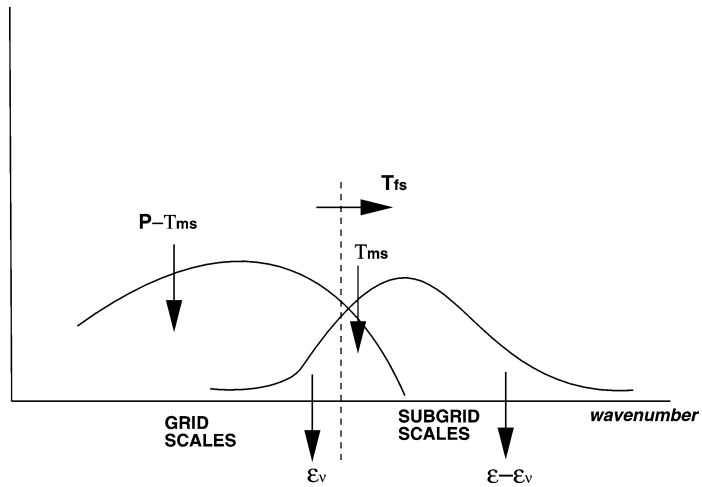

Fig. 4. Schematic diagram of the energy spectrum at low Reynolds numbers. Production and separation are not well separated. Production, T^{MS}, occurs in the subgrid scales and direct viscous dissipation, ε_v, occurs in the resolved scales so that $T^{FS} < \varepsilon$.

the Gaussian filter,

$$\widehat{G}_i = \mathrm{e}^{-k^2\Delta_i^2/24}; \tag{27}$$

and the box filter,

$$G_i = \begin{cases} 1/\Delta_i & \text{if } |x_i| \leqslant \Delta_i/2, \\ 0 & \text{otherwise.} \end{cases} \tag{28}$$

Here $\widehat{G}_i$ is the Fourier coefficient of the filter function in the ith direction, $K_i = 2\pi/\Delta_i$ is the cutoff wavenumber, and Δ_i is the filter width in the ith direction. In what follows, three cutoff wavenumbers are chosen, summarised in Table 1. Inspection of Fig. 1 shows that these lie in the $-5/3$ region.

The different types of filter have nominally the same widths, so that the effect of filter shape can be determined independently of the effect of filter size; Lund [36] discusses how the width of a filter should be determined. Härtel and Kleiser [37] suggest that when a filter other than the cutoff filter is used, the Leonard and cross stresses will both contain Galilean-invariant components which cancel out if these quantities are summed. Since in the present work the subgrid stresses are analysed as a whole, and not as individual components, then the effects of Galilean invariance are removed.

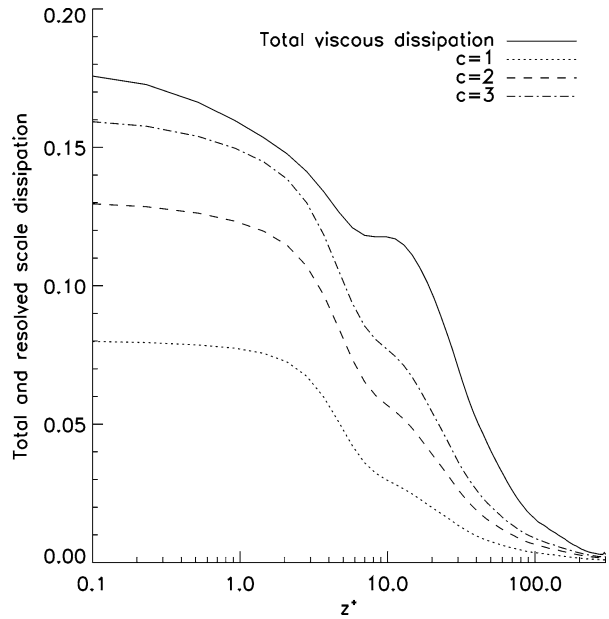

Fig. 5. Effect of filter width on resolved-scale dissipation, ε_ν^+; cutoff filter; $Re_\delta = 300$.

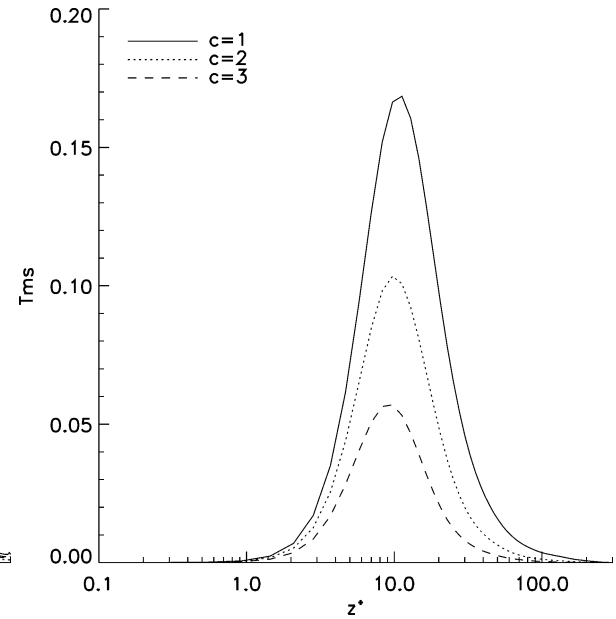

Fig. 6. Effect of filter width on T^{MS+}; cutoff filter; $Re_\delta = 300$.

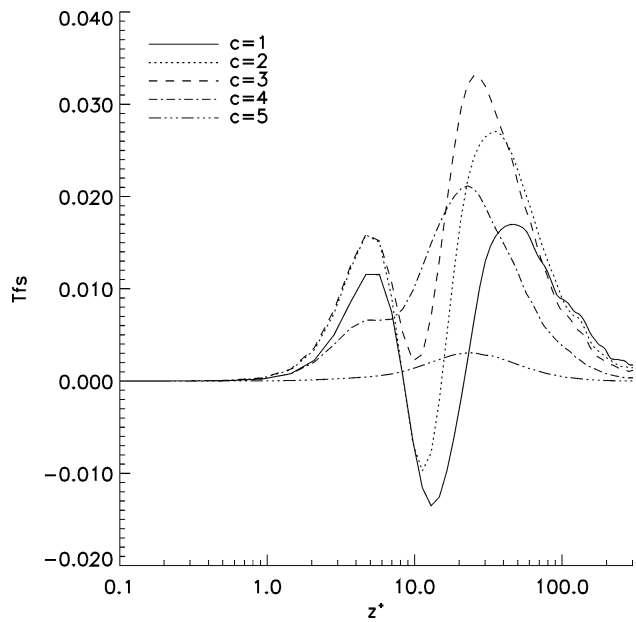

Fig. 7. Effect of filter width on T^{FS+}; cutoff filter; $Re_\delta = 300$.

In order to illustrate the relationship between the filters and the spectra, the filter shapes are plotted against k^* in Fig. 2. η has been calculated for $z^+ = 68$. At higher values of z^+, the values of non-dimensionalised wavenumber at which the filter cutoffs occur will be slightly greater as η increases. Here, we define a filter "width" to be a width in wavenumber space for the three filters defined above. All the filtering is carried out in Fourier space, using two-dimensional fast Fourier transform routines, in homogeneous planes parallel to the wall. Explicit filtering in the wall-normal direction has not been carried out. Murray et al. [26] show that two-dimensional filtering in planes parallel to the wall is equivalent to three-dimensional filtering above $z^+ \simeq 10$.

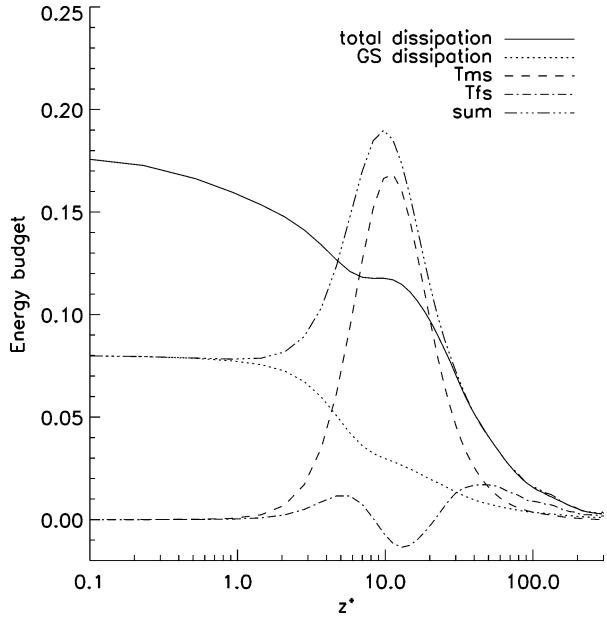

Fig. 8. Energy budget scaled on wall units; cutoff filter, $c = 2$; $Re_\delta = 300$.

6. Analysis of the energy budget at low Reynolds number

In order to investigate low-Reynolds-number effects, terms representing different processes in the energy budget are considered. Following the analysis of Härtel et al. [3], the subgrid-scale transfer is separated into two contributions,

$$T = T^{MS} + T^{FS}, \tag{29}$$

where

$$T^{MS} = \langle \tau_{ij} \rangle \langle \widetilde{S}_{ij} \rangle, \tag{30}$$

and

$$T^{FS} = \langle \tau'_{ij} \widetilde{S}'_{ij} \rangle. \tag{31}$$

The term T^{MS} represents an enhancement of the subgrid scales due to the mean shear, and is the contribution to the energy production by the subgrid scales. T^{FS} represents a redistribution of kinetic energy within the turbulence spectrum. Thus, in the ideal high-Reynolds-number large-eddy simulation (as the model requires):

$$T^{FS} = \varepsilon, \qquad T^{MS} = 0, \qquad \varepsilon_\nu = 0, \tag{32}$$

where $\varepsilon_\nu = \nu \langle \widetilde{S}'^2_{ij} \rangle$ is the mean viscous dissipation effected by the resolved scales. Schematic diagrams representing the relationship between terms in the energy budget and the energy spectra are shown in Figs. 3 and 4 for the high and low Reynolds number cases. In the low-Reynolds-number case, the dissipation is also effected by the resolved scales, ε_ν, as well as the subgrid scales. Thus, in general, the energy budget is given approximately by:

$$\varepsilon \approx \varepsilon_\nu + T^{MS} + T^{FS}. \tag{33}$$

This relation becomes exact in the case of the Fourier cutoff filter and in the absence of transport which provides additional sources or sinks at each wavenumber. For either the Gaussian filter, or the box filter, it is only ever approximate, even when transport is zero. Low-Reynolds-number effects cause a decrease in the value of T^{FS} relative to ε. Bradshaw's [33] criterion for a "first-order" subrange suggests that, in order to optimise the analysis of low-Reynolds-number DNS data for emulating a high-Reynolds-number large-eddy simulation, one should select the filter width (in wavenumber space) which gives the maximum value of T^{FS}. Then the combined effects of production by the subgrid scales and dissipation by resolved scales are minimised. However, because T^{FS} varies rapidly with z^+ and may take either sign, the optimum filter width will always depend to some extent on z^+.

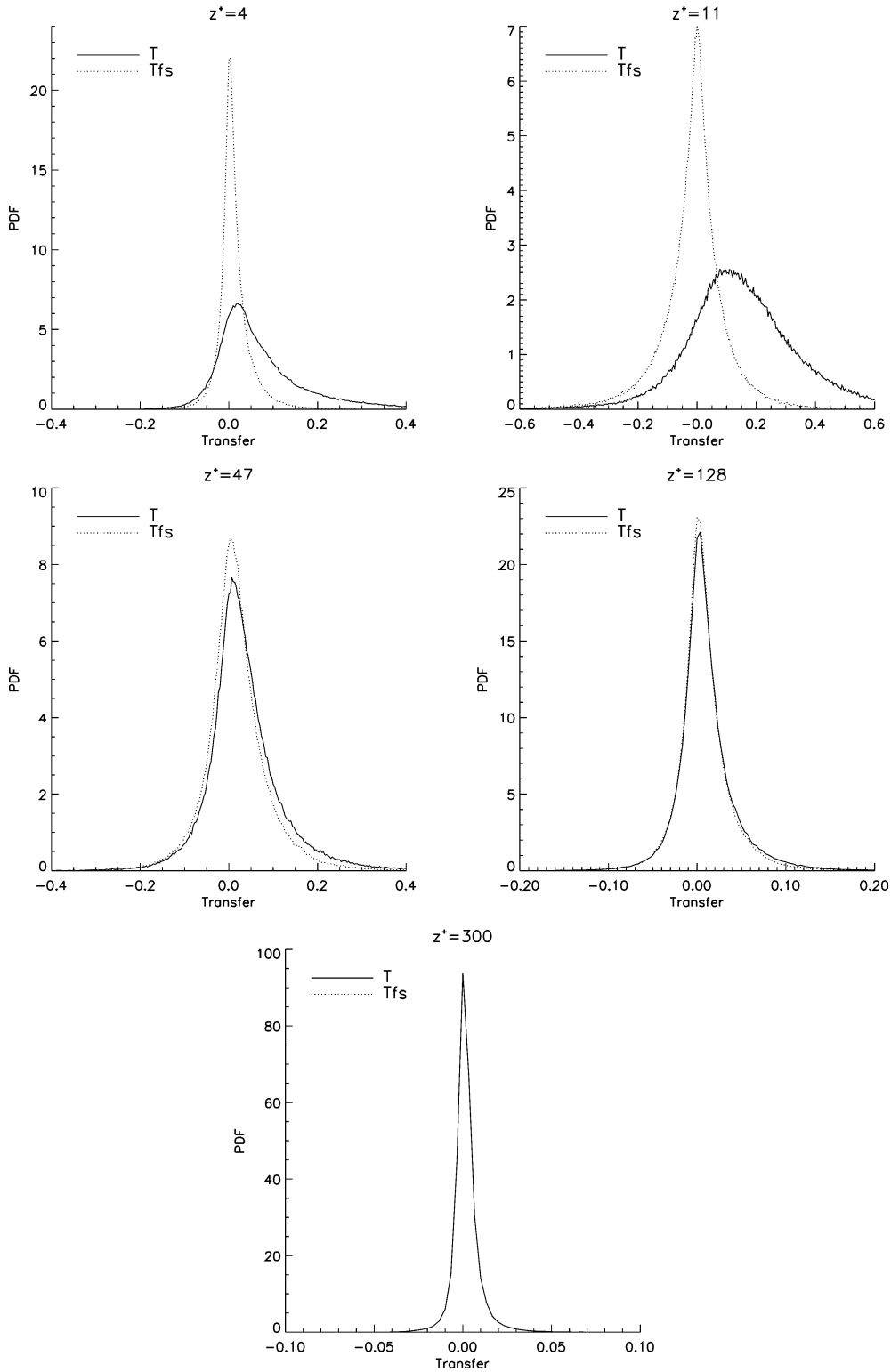

Fig. 9. Pdf's of T^{+} and T^{FS+} at different values of z^{+}.

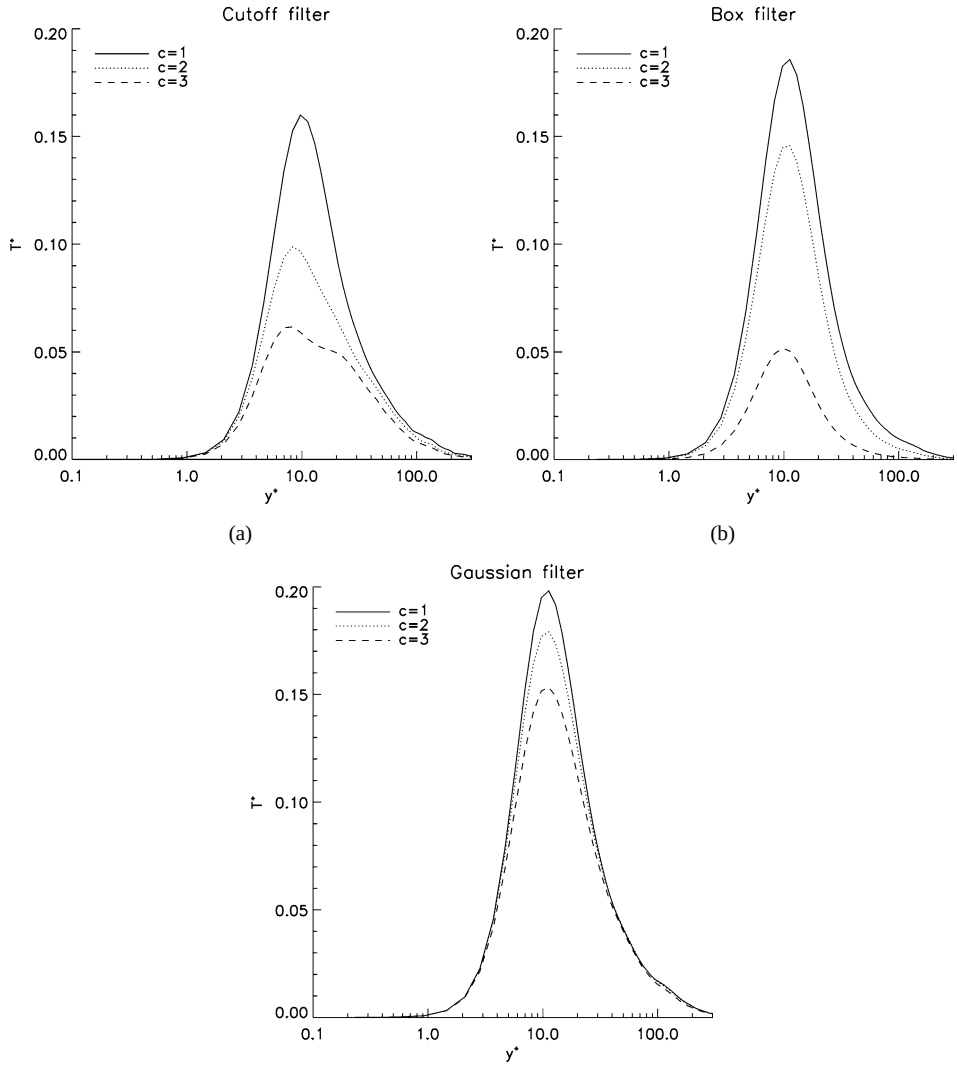

Fig. 10. Effect of filter on profiles of energy transfer, T^+: (a) cutoff; (b) box and (c) Gaussian filters.

The extent to which the viscous dissipation is effected by the resolved scales is illustrated in Fig. 5, where ε_ν^+, evaluated using cutoff filters of different widths (see Fig. 2, and Table 1), is plotted with ε^+. Even at the narrowest filter width, there is a significant contribution to the viscous dissipation by the resolved scales throughout the channel. The effect of filter width on the production of energy by the subgrid scales, T^{MS+}, is shown in Fig. 6 for the cutoff filter. In the near-wall region, there is a significant contribution to the production by the subgrid scales, even when the cutoff is placed towards the high-wavenumber end of the $-5/3$ region. At all filter widths, however, T^{MS} is negligible in the flow interior where the mean strain rate is small, and most of the energy-producing scales are resolved.

The effect of cutoff filter width on the energy transfer due to the fluctuating rate of strain, T^{FS+}, is shown in Fig. 7. The shapes of the profiles are very similar to those in Härtel et al. [3], and illustrate that, for the narrower filters, there is significant backscatter for $z^+ \approx 15$. Also shown is T^{FS} for two wider filters, denoted $c = 4$, $c = 5$ and which are, respectively, two and four times wider than the $c = 3$ case. If a much wider filter is used, backscatter is not apparent. At $z^+ \approx 30$, there is a clear trend in the profiles: T^{FS} increases with increasing filter width, reaches a maximum for $c = 3$, after which it decreases. At smaller z^+, the trend is clear for the narrower filter widths, but not for the wider filters, where the value of T^{FS} continues to increase. Overall, this behaviour suggests that the optimum filter width is provided by $c = 2$, for which there is significant backscatter and forward scatter and T^{MS} and ε_ν are small at suitably large z^+. Fig. 2 shows that $c = 2$ occurs in the middle of the $-5/3$ range of wavenumbers, $k^* = 0.088$.

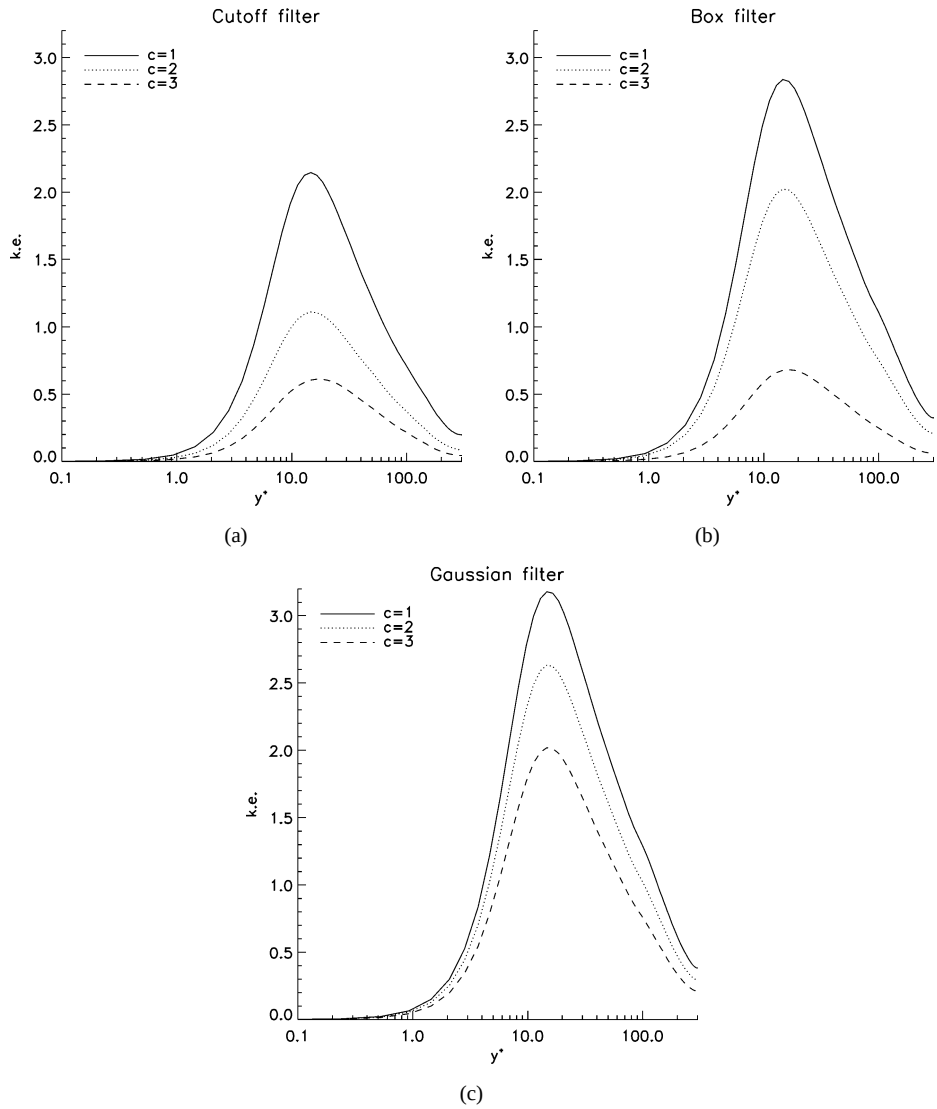

Fig. 11. Effect of filter on profiles of subgrid energy, τ_{kk}: (a) cutoff; (b) box and (c) Gaussian filters.

In Fig. 8, the constituent terms of Eq. (33) are plotted together with their sum at the optimum cutoff filter width, $c = 2$. The sum of components is very similar to ε for $z^+ \geqslant 25$ only. This is due to the viscous diffusion which is significant for $z^+ \leqslant 20$. Additionally, two-dimensional filtering becomes an inaccurate approximation to three-dimensional filtering for $z^+ < 10$ [26]. This analysis shows that, in the viscous sublayer, T^{MS} and ε_ν are significant. At the much higher Reynolds numbers typical for LES, the relative magnitudes of these terms will remain approximately the same when scaled on wall units. However, in dimensional terms, the proportion of the channel over which T^{MS} and ε_ν are significant decreases with increasing Reynolds number, as the separation of the energy-producing and energy-dissipating scales becomes more distinct. Thus at much higher Reynolds numbers, it is expected that the energy transfer, T, will be a result of only the difference between the true forward scatter and backscatter over a larger fraction of the layer. Typically, Mason and Thomson [15] indicate that the first mesh point in their LES is typically at 5 m, equivalent to $z^+ \approx 10^5$.

7. Analysis of the energy transfer, T

A more detailed comparison between T^{FS+} and T^+ is provided by an inspection of the unfiltered probability distribution functions (pdf's). These are scaled so that the area under the curve is equal to unity. These are shown in Fig. 9 for five different

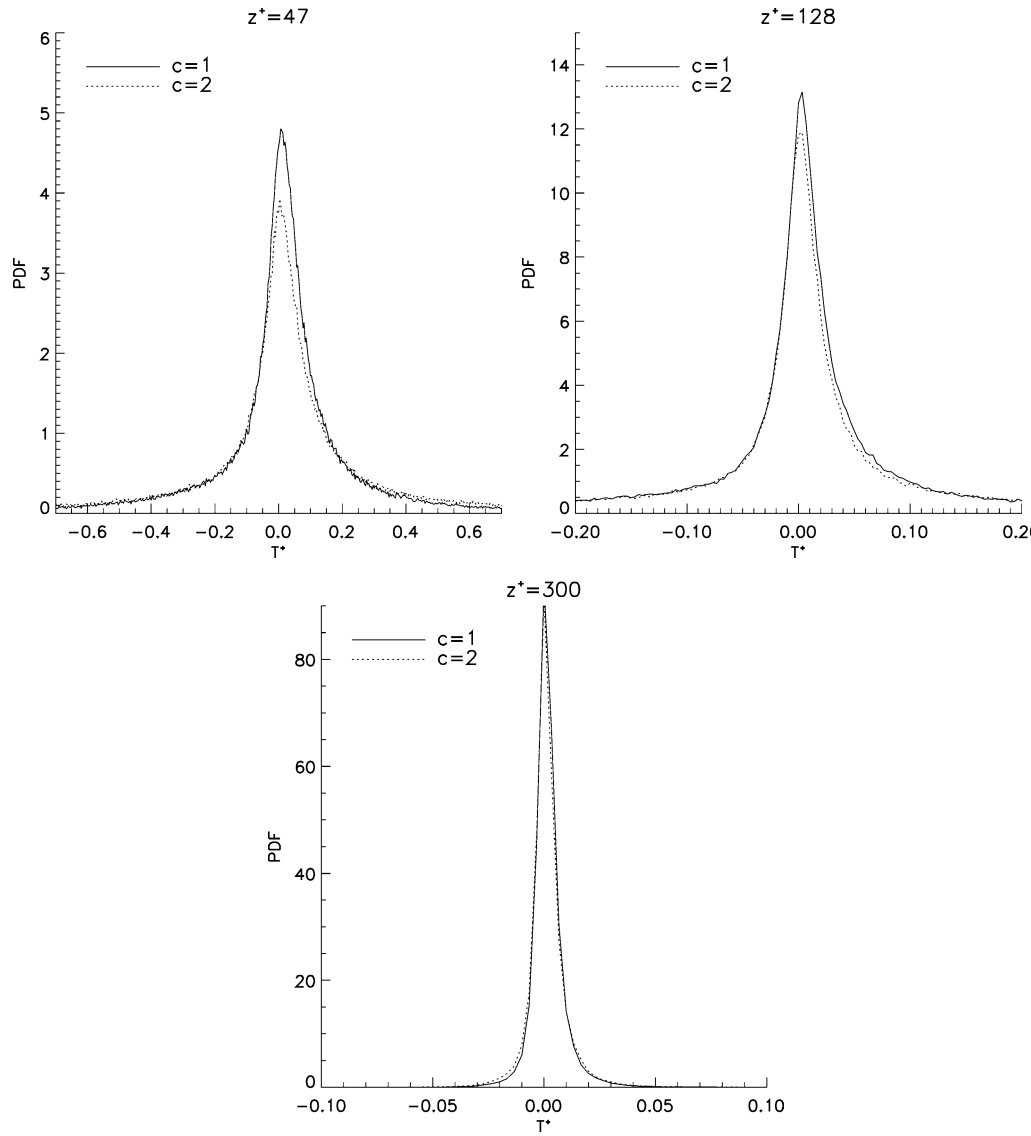

Fig. 12. Effect of filter width on PDFs of T^+; cutoff filter.

values of z^+. They are markedly different only for $z^+ < 50$, above which it seems reasonable to model the energy transfer T as a whole, rather than using T^{FS}. Note that T^{FS+} is positively skewed at all positions except at $z^+ = 11$ where the backscatter is greatest. Interestingly, T^+ is positively skewed at all positions. Nearer the wall, it may be better to consider the terms T^{MS} and T^{FS} separately in order to create a model with a sounder physical basis, since they represent different physical processes. However, correct modelling of both T^{MS} and T^{FS} relies on the accurate representation of the subgrid stresses, since these terms arise through interactions of the subgrid stresses with the mean and fluctuating strain rates, respectively. Thus, it is possible that both quantities might be adequately modelled by stochastic fluctuations.

7.1. Effects of filter shape and size

Owing to the inherent uncertainties associated with the effective filter shape in implicit filtering, a brief comparison of the three filters is now made. The effects of filter width and shape are shown in Fig. 10, where profiles of T evaluated using the cutoff filter, box filter and Gaussian filter have been plotted. The profiles for the cutoff and box filters are similar to those in Piomelli et al. [5]

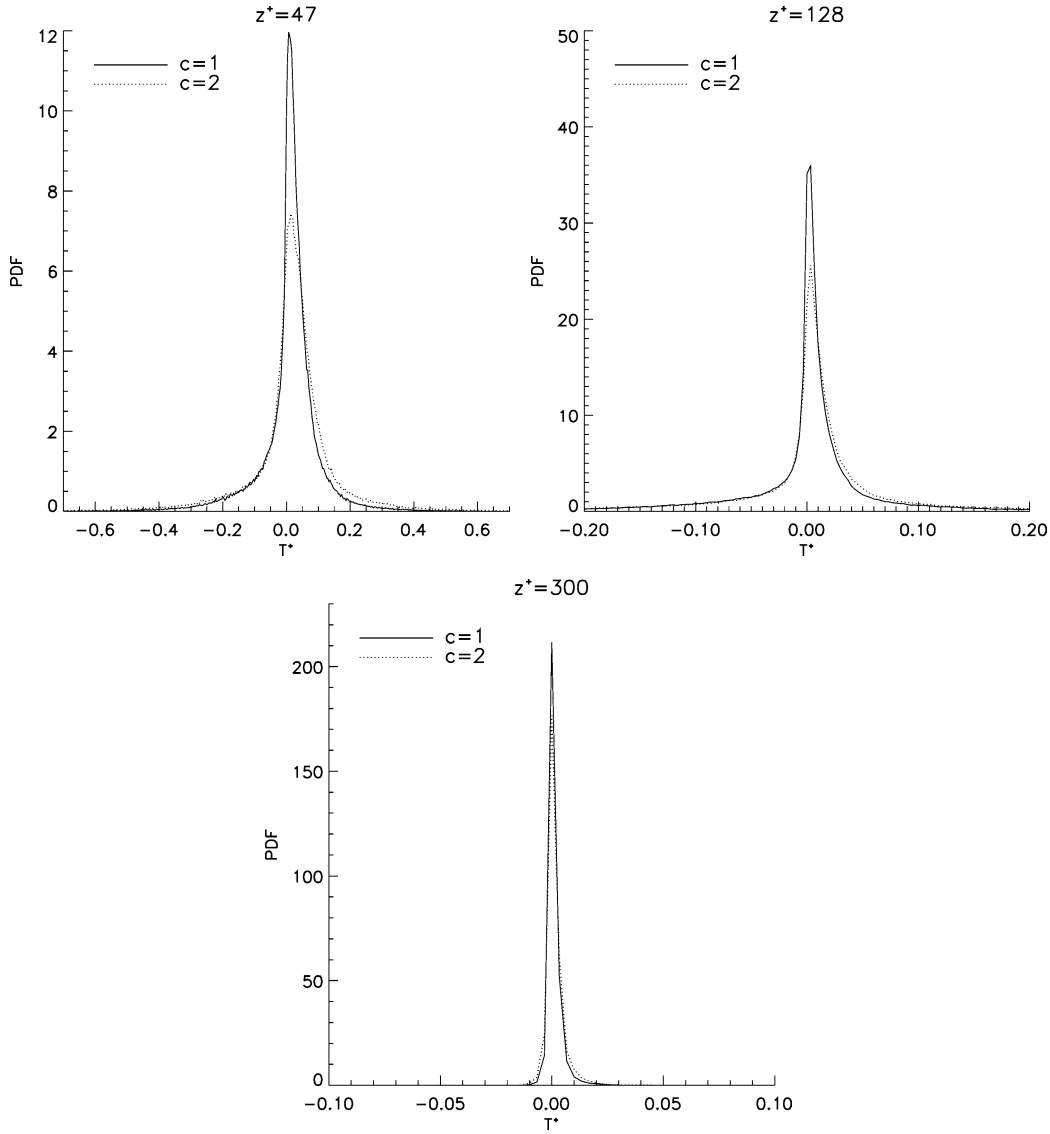

Fig. 13. Effect of filter width on PDFs of T^+; box filter.

The profiles show that the net energy transfer is greatest near $z^+ = 10$, where the production of turbulent kinetic energy is at a maximum, and decreases towards the interior of the flow. The magnitude of T^+ decreases as the filter width increases. There is a corresponding decrease in the subgrid energy (Fig. 11) as the filter width increases, since the proportion of scales which are below the cutoff is decreasing. T^+ is greater for the box and Gaussian filters than the cutoff filters at approximately equivalent widths. This is because the box and Gaussian filters begin to drop off in Fourier space at wavenumbers below the cutoff, and therefore they filter out a greater proportion of the energy contained in the large scales. This effect is also illustrated by the profiles of subgrid energy.

Probability distributions of T^+ are plotted for the Fourier cutoff, box and Gaussian filters in Figs. 12, 13 and 14, respectively. For each filter type, pdf's are shown for filters $c = 1$ and $c = 2$ at $z^+ = 47$, 128 and 300. In order to make these results as relevant as possible to the Mason and Thomson model, the value of $z^+ = 47$ is taken to be the lowest position as this is the one at which there is reasonable agreement between the pdf's of T^+ and T^{FS+}. At each value of z^+, the pdf's have been plotted with the same x-axis range for the different filter types for ease of comparison. For the cutoff and box filters, the peak value of the pdf decreases as the filter width (in wavenumber space) increases. For the Gaussian filter, the opposite occurs. These changes are most marked at $z^+ = 47$. In all three cases, the effect of increasing filter width is to reduce the mean. Yet, only in the cases of

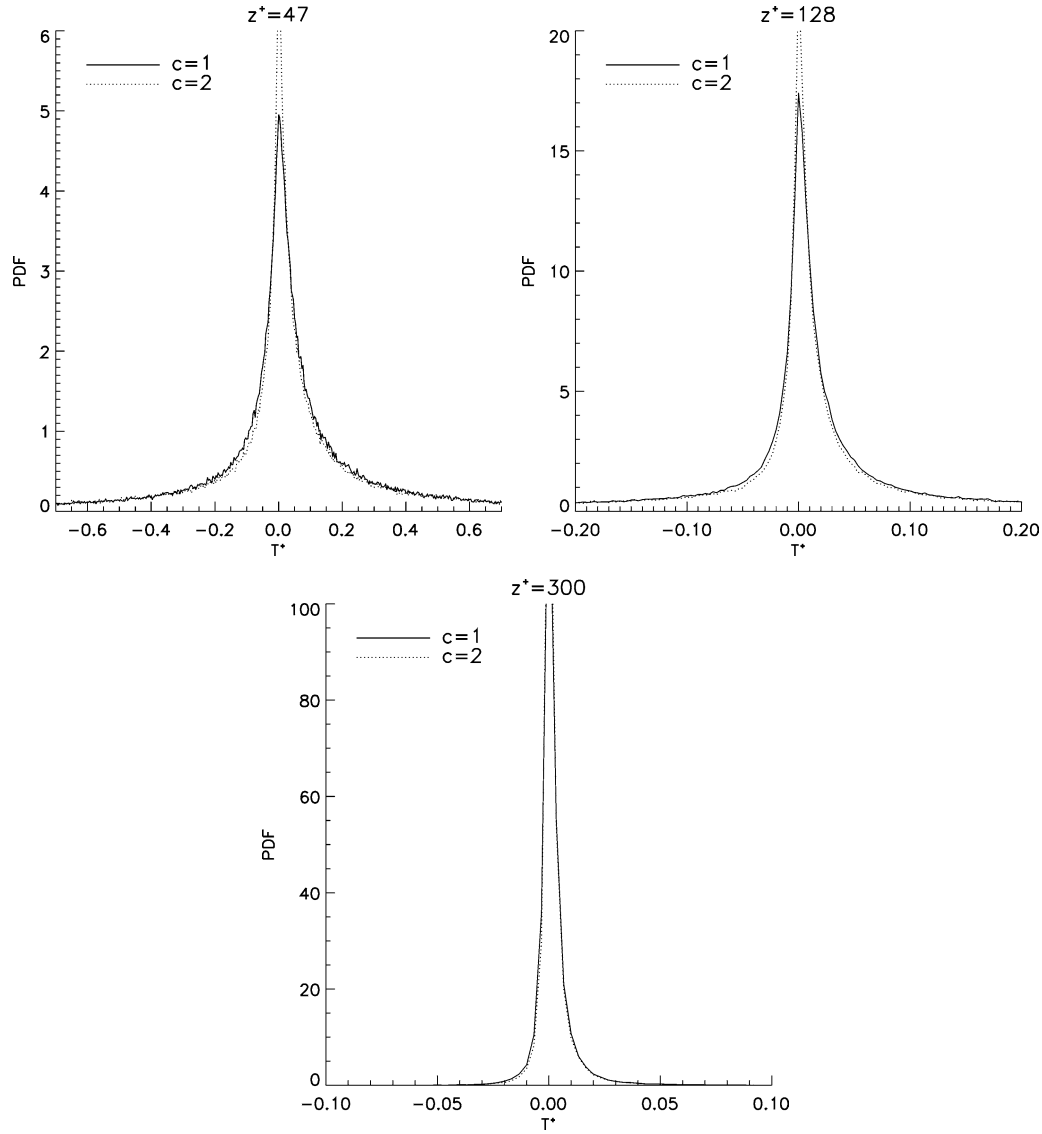

Fig. 14. Effect of filter width on PDFs of T^+; Gaussian filter.

the box and Gaussian filters does this correspond to a decrease of the variance; for the cutoff filter, the variance increases. As the filter width increases, the transfer from resolved scales to subgrid scales ($T^{FS} \approx T$) occurs at higher wavenumbers. This appears to produce a greater proportion of instantaneous energy transfers with smaller magnitude. It is evident that the variance for all filters decreases as z^+ increases. The variances for the cutoff filters are larger than those for the box and Gaussian filters. Real-space quantities such as T defined using a Fourier-space filter will lead to negative filter values within the oscillations exhibited by the cutoff filter in real space. This produces unphysical effects, while the box and Gaussian filters have similar transfer functions for real-space quantities. Owing to the similarity between the Gaussian and box-filter statistics, the former are not considered further.

7.2. PDF's of energy transfer conditional on the strain rate squared

Contours of the joint pdf of energy transfer, T^+, and normalised strain rate squared, $\widetilde{S}_{ij}^{2+}$, are plotted in Fig. 15 for the cutoff filter, $c = 1$. The distributions are not normalised; instead, they show the number of points with certain values of T^+ and $\widetilde{S}_{ij}^{2+}$ such that the area under the envelope of the contours sums to unity. They are generated over three timesteps separated by ten

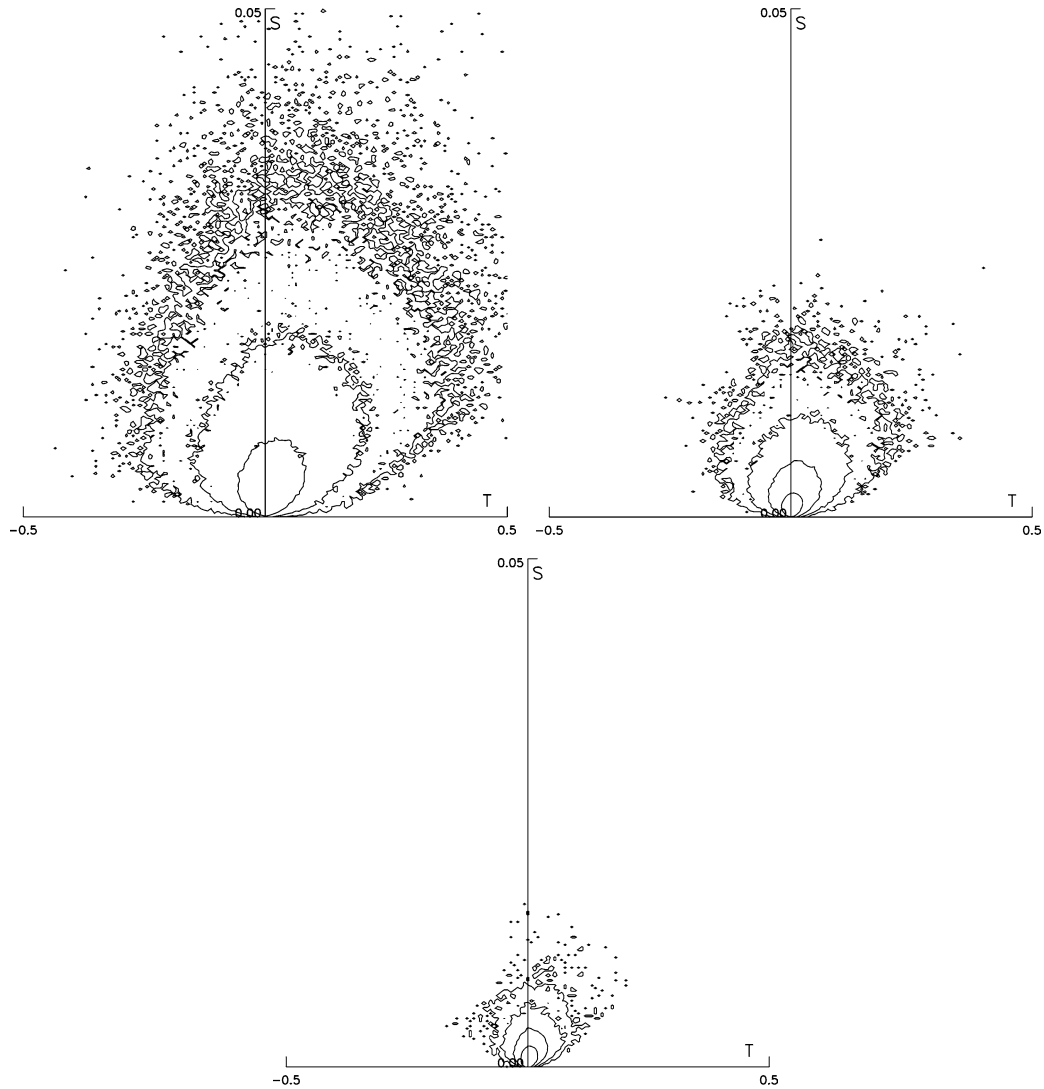

Fig. 15. Contours of joint pdf's of energy transfer, $T^+/\widetilde{S}_{ij}^{2+}$; cutoff filter $c = 1$. (a) $z^+ = 47$; (b) $z^+ = 128$; (c) $z^+ = 300$; contour values, 0.1, 1.0, 10, 100.

eddy turnover times, to provide reasonably smooth distributions. They show that, as is commonly accepted, the subgrid-scale stresses cannot be determined uniquely from the resolved strain rate squared, since for one value of $\widetilde{S}_{ij}^{2+}$, there is a range of possible values of T^+. Thus the usual Smagorinsky model equation linking the strain rate to the subgrid stresses (Eq. (9)) is unlikely to be adequate. As $\widetilde{S}_{ij}^{2+}$ increases, the variances of the probability distributions increase. This is in agreement with the equation for the modelled probability distribution (Eq. (22)), in which the variances of the generated distributions are proportional to $\widetilde{S}_{ij}^{3}$. This suggests that there is a reasonably sound basis to the model.

7.3. Model PDF's of energy transfer, T

The probability distributions of modelled energy transfer, evaluated using Eq. (22), are plotted in Fig. 16, for the cutoff filter, $c = 1$ at each of the three planes, $z^+ = 47, 117$ and 180. For comparison, the distributions obtained directly from the DNS data are also plotted. The modelled distributions have been evaluated using three values of the tuneable constant, $0.3 \leqslant a \leqslant 0.5$. In order to minimize the number of free constants, the value of the constant C_B has been kept at the same value of 1.4 for all values of z^+, and has not been adjusted according to Eq. (24). Therefore the model pdf's can be expected to have greater validity away

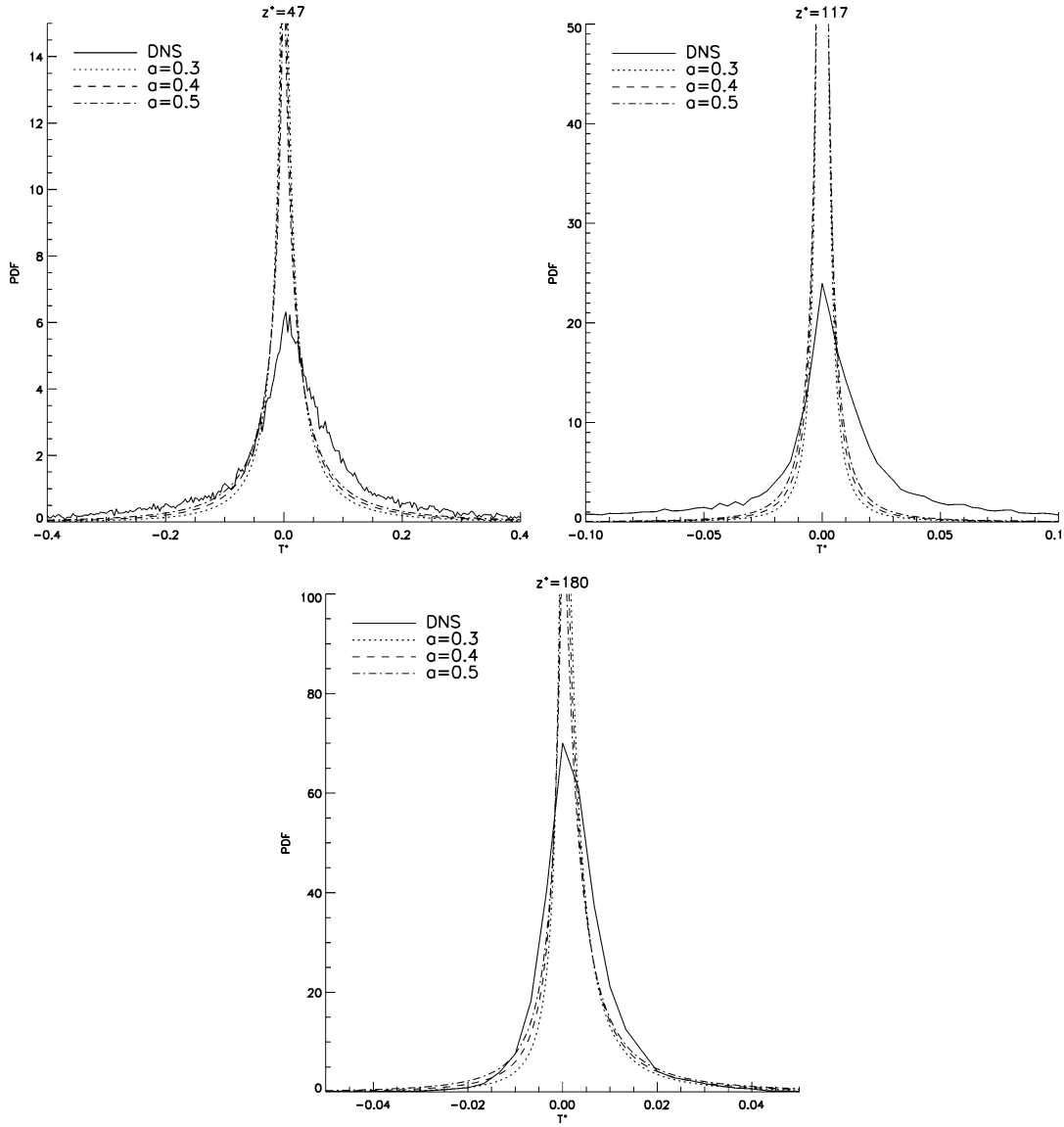

Fig. 16. Comparison between model pdf's of T and pdf's from DNS data; cutoff filter, $c = 1$. (a) $z^+ = 47$; (b) $z^+ = 117$; (c) $z^+ = 180$.

from the surface. Similarly, the value of the length scale, l, is not calculated using Eq. (23); rather, l is chosen so that the first term of Eq. (22) is matched to the mean transfer calculated from the DNS data. The values of l evaluated in this way have a smaller magnitude than if Eq. (23) were used. Also, it is found that the filter width, $l_f > l/0.2$. This procedure means that a may be adjusted to optimise agreement between the model and DNS variances. The pdf moments are shown in Table 2. The corresponding distributions for the box filter, $c = 1$, are plotted in Fig. 17, and their moments are given in Table 3. For the box filter, $0.2 \leqslant a \leqslant 0.4$.

It should be expected that the model distributions are most likely to match the DNS distributions away from the surface: those for $z^+ = 180$ show that this is the case, for both filters of width, $c1$. This is also the case for both filters of width, $c2$ (not shown). Generally, the agreement between the variances is better in the case of the box filter and this agreement improves as z^+ increases, or equivalently, the variance of the DNS data decreases. The optimum value of a increases as the distance to the surface decreases, while it might be be expected that a should decrease in order to allow for a decrease in the value of the constant, C_B, in Eq. (24). However, the actual changes in pdf of the DNS data with z^+ are rather more complicated. The most significant difficulty lies in the insensitivity of the model to changes in a for the planes used here. For both filters, the decrease in optimum value of a between $z^+ = 47$ and $z^+ = 180$ is not monotonic: the apparent optimum value of a at $z^+ = 117$ is many

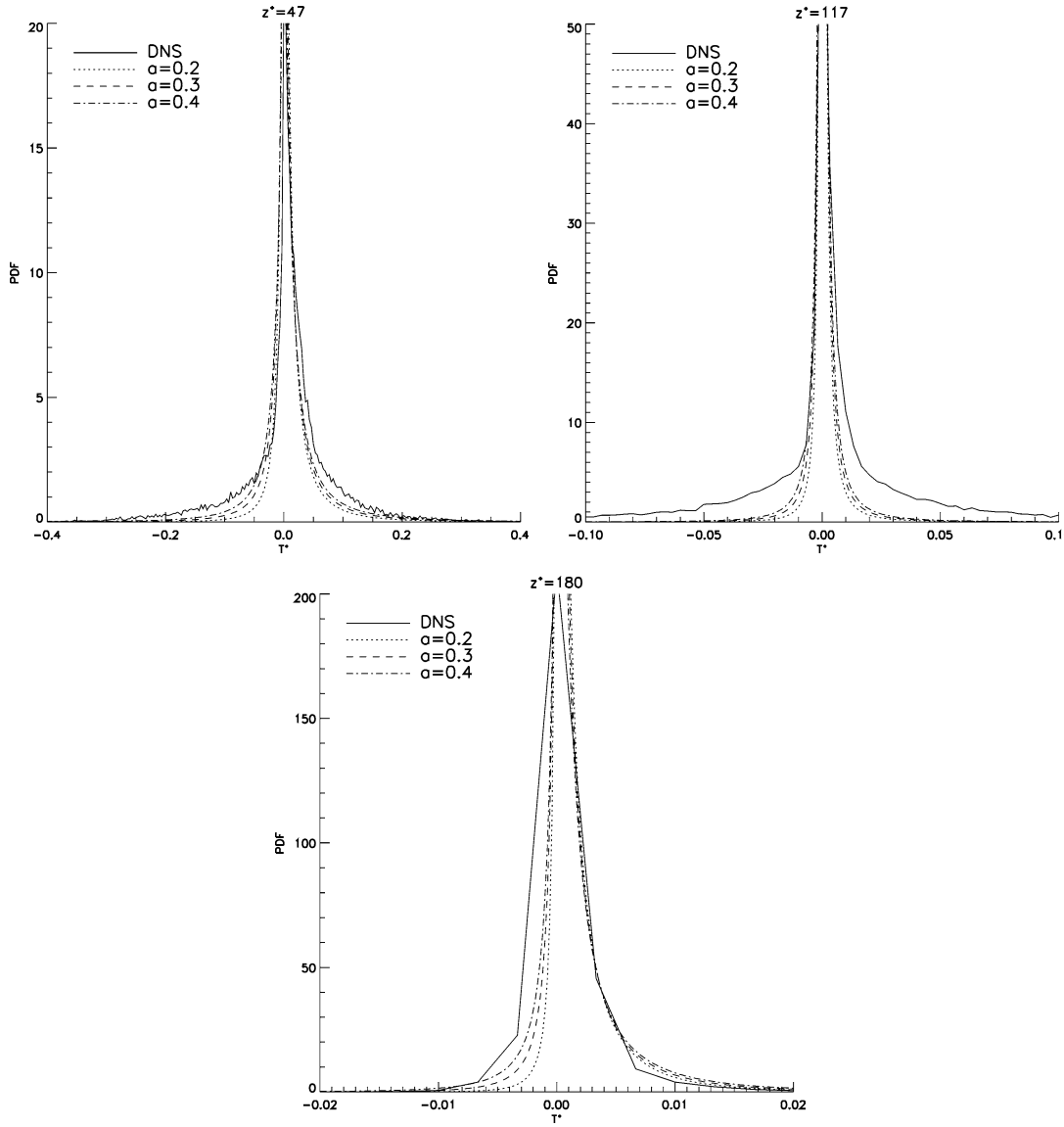

Fig. 17. Comparison between model pdf's of T and pdf's from DNS data; box filter, $c = 1$. (a) $z^+ = 47$; (b) $z^+ = 117$; (c) $z^+ = 180$.

times the values required at the other two heights. This issue is not really important at the much larger values of z^+ at which the model is likely to be applied. The higher moments show a further, related difficulty: the actual pdf's are much more non-Gaussian than the model suggests and the model is unable to predict the large changes in skewness which is negative at $z^+ = 47$ and 117, but positive at $z^+ = 180$. In general therefore, the model places undue emphasis on transfers of small magnitude and the actual transfers are significantly more bi-directional in nature.

8. Discussion and conclusions

DNS databases of turbulent channel flow at $Re_\delta = 300$ have been used to analyse the energy transfer between resolved and subgrid scales. The use of low-Reynolds-number data has important implications for their analysis [3,19]: the energy transfer, T, contains components T^{MS} and T^{FS} which arise from the interactions of the subgrid stresses with the mean and fluctuating strain rates, respectively. At the meteorological Reynolds numbers at which the Mason and Thomson model is applied, T^{MS} will be negligible at large z^+ and $T^{FS} \simeq \varepsilon$. Similarly, the resolved-scale dissipation, $\varepsilon_\nu \simeq 0$ away from the surface.

Table 2
Moments of pdf's of energy transfer, T: DNS data and Mason and Thomson model; cutoff filter, c1

	a	Mean	Variance	Skewness	Flatness
$z^+ = 47$	DNS data	6.71×10^{-3}	6.40×10^{-2}	-1.51	1.55×10^{3}
	0.3	6.70×10^{-3}	9.52×10^{-3}	-1.77	81.7
	0.4	6.67×10^{-3}	1.65×10^{-2}	-1.20	68.7
	0.5	6.62×10^{-3}	2.49×10^{-2}	-0.842	56.8
$z^+ = 117$	DNS data	3.25×10^{-4}	3.17×10^{-2}	-19.9	1.12×10^{4}
	0.3	3.25×10^{-4}	2.06×10^{-4}	-1.56	2.11×10^{2}
	0.4	3.25×10^{-4}	3.63×10^{-4}	-1.12	2.00×10^{2}
	0.5	3.23×10^{-4}	5.55×10^{-4}	-0.822	1.79×10^{2}
$z^+ = 180$	DNS data	3.03×10^{-3}	1.73×10^{-4}	3.91×10^{5}	5.77×10^{8}
	0.3	3.03×10^{-3}	3.21×10^{-5}	-3.51	53.2
	0.4	3.03×10^{-3}	4.64×10^{-5}	-2.73	49.4
	0.5	3.02×10^{-3}	6.64×10^{-5}	-3.16	43.7

Table 3
Moments of pdf's of energy transfer, T: DNS data and Mason and Thomson model; box filter, c1

	a	Mean	Variance	Skewness	Flatness
$z^+ = 47$	DNS data	1.03×10^{-2}	1.12×10^{-2}	-3.06×10^{2}	6.57×10^{4}
	0.2	1.03×10^{-2}	1.56×10^{-3}	-3.44	35.7
	0.3	1.03×10^{-2}	3.15×10^{-3}	-2.57	34.7
	0.4	1.03×10^{-2}	5.37×10^{-3}	-2.02	34.1
$z^+ = 117$	DNS data	6.64×10^{-3}	4.86×10^{-3}	-2.96×10^{3}	5.96×10^{5}
	0.2	6.60×10^{-4}	4.91×10^{-5}	-7.46	2.46×10^{2}
	0.3	6.62×10^{-4}	1.04×10^{-4}	-5.31	2.40×10^{2}
	0.4	6.63×10^{-4}	1.81×10^{-4}	-4.07	2.37×10^{2}
$z^+ = 180$	DNS data	1.70×10^{-3}	2.89×10^{-5}	1.93×10^{7}	2.26×10^{10}
	0.2	1.70×10^{-3}	1.26×10^{-5}	-4.94	47.7
	0.3	1.70×10^{-3}	1.97×10^{-5}	-4.61	50.9
	0.4	1.70×10^{-3}	2.97×10^{-5}	-4.07	51.3

An examination of the DNS data shows that, for $z^+ > 50$, T^{MS} is negligible so that $T \simeq T^{FS}$. Detailed analysis of the pdf's of energy transfer, T, have been performed and compared with those generated using the Mason and Thomson stochastic backscatter model with the first moment matched to the value of T given by the DNS data. Using a single tuneable constant to match the variances, the model reproduces pdf's of roughly the correct shape, except that the magnitudes of the skewness and flatness are significantly underestimated. The model appears to be insufficiently sensitive to the details of the energy transfer even at large z^+ where it is supposed that the model will work well. The difficulty arises in the term, $|\nabla \wedge u_i|$, in the model, Eq. (22), that represents the physical influence of the turbulence. This is the curl of the velocity or vorticity. However, Dunn and Morrsion [22] have recently shown that it is the non-linear term which is the most intermittent, and therefore the term in the equations of motion that is responsible for the large skewness and flatness of the transfer term. A possible improvement to the model might therefore be to replace this term with one of the form, $u_j \partial u_i / \partial x_j$, which would enable a better shape of pdf to be generated. In turn, this would make it easier to optimise the model by using as few constants as possible. This becomes even more important at small z^+ where the net transfer is the small difference between forward scatter and backscatter, both of large magnitude but of opposite sign. The development of a similar stochastic model for T^{ms} would enable the use of the backscatter model at smaller z^+.

In dealing with real-space quantities such as T (and the backscatter model is defined in real space also), it appears that the box filter describes better the effective filter produced by the implicit filtering of the Mason and Thomson [15] LES code. This is in agreement with the suggestion by Meneveau [8]. By comparison, the cutoff filter places undue emphasis on transfers of small magnitude that are caused by a real-space reduction of filter amplitude at displacements less than $\pi/2K_i$.

Fig. 9 shows that, in the viscous sublayer, the pdf's of T^{FS} are significantly non-Gaussian, the sign of the skewness largely determining the sign of the mean. Thus at $z^+ = 5$, both the first and third moments are positive, while at $z^+ = 11$, they

are both negative. It is therefore likely that the backscatter model would not perform well in the sublayer, although a much more important issue is the inadequacy of the log law as an "off-the-wall" surface boundary condition, as used by Mason and Thomson [15]. This problem has not yet been fully addressed, although recent attempts have been made [38]. The inadequacy of the Smagorinsky model is illustrated further by the probability distributions of energy transfer conditional on $\widetilde{S}_{ij}^{2+}$. These show that the subgrid stresses cannot simply be related to the resolved strain rate, since for one value of $\widetilde{S}_{ij}^{2+}$, a range of values of T^+ are possible. However, the variances of the pdf's increase with increasing $\widetilde{S}_{ij}^{2+}$, which is in agreement with the Mason and Thomson backscatter model.

A further question that remains unanswered is the relevance of the present results obtained using low-Reynolds-number data to the meteorological Reynolds numbers at which the stochastic backscatter model is applied. Even with the analysis that separates T^{fs} from T, it is likely that energy transfer mechanisms in the wall region do not scale simply with Reynolds number. Recent experimental evidence [39] suggests that the peak of energy production near $z^+ \approx 15$ increases with Reynolds number when scaled on wall units. This implies that spectral transfer further from the surface does also, and that this outer-layer, "top–down" effect contributes to the near-surface dynamics. Owing to the way in which the model pdf's were generated by matching the first moment to that of the DNS data, the single free constant will not have relevance to the model constants when used in *a posteriori* tests at high Reynolds number. The implication is that, because of the very large changes in the higher moments of the actual transfer with height, the first moment that would be predicted in such tests will also be similarly sensitive. Therefore an attempt at improving the model in predicting the skewness as suggested above is a logical next step. Further development should surely involve the effects of surface roughness intrinsic to the near-surface behaviour of geophysical boundary layers.

Acknowledgements

We are indebted to the Meteorological Office, Exeter, for financial support under Agreement Met. 1b/2126, and to EPSRC for support under grant GR/M31187/01. The work has greatly benefited from discussions with Dr. David Thomson. We are also indebted to Professor Neil Sandham of Southampton University for access to the DNS databases generated under the auspices of the UK Turbulence Consortium (EPSRC GR/M08424, GR/R26368 & GR/R64957).

References

[1] P. Spalart, Stategies for turbulence modelling and simulations, Int. J. Heat and Fluid Flow 21 (2000) 252–263.
[2] J. Jiménez, R.D. Moser, Large-eddy simulations: where are we and what can we expect?, AIAA J. 38 (2000) 605–612.
[3] C. Hărtel, L. Kleiser, F. Unger, R. Friedrich, Subgrid-scale energy transfer in the near-wall region of turbulent flows, Phys. Fluids 6 (1994) 3130–3143.
[4] U. Piomelli, P. Moin, W.H. Cabot, S. Lee, Subgrid-scale backscatter in turbulent and transitional flows, Phys. Fluids 3 (1991) 1766–1771.
[5] U. Piomelli, Y. Yu, R.J. Adrian, Subgrid-scale energy transfer and near-wall turbulence structure, Phys. Fluids 8 (1996) 215–224.
[6] K. Horiuti, Backward scatter of subgrid-scale energy in wall-bounded and free shear turbulence, J. Phys. Soc. Japan 66 (1997) 91–107.
[7] J.A. Domaradzki, W. Liu, C. Hărtel, L. Kleiser, Energy transfer in numerically simulated wall-bounded turbulent flows, Phys. Fluids 6 (1994) 1583–1599.
[8] C. Meneveau, Analysis of turbulence in the orthonormal wavelet representation, J. Fluid Mech. 232 (1991) 469–520.
[9] J. Smagorinsky, General circulation experiments with the primitive equations: 1. The basic experiment, Mon. Weather Rev. 91 (1963) 99–164.
[10] J. Bardina, J.H. Ferziger, W.C. Reynolds, Improved turbulence models based on large eddy simulation of homogeneous, incompressible, turbulent flows, Technical Report Report No. TF-19, Thermosciences Division, Department of Mechanical Engineering, Stanford University, 1983.
[11] P.J. Mason, A.R. Brown, The sensitivity of large-eddy simulations of turbulent shear flow to subgrid models, Boundary-Layer Meteorology 70 (1994) 133–150.
[12] A. Muschinski, A similarity theory of locally homogeneous and isotropic turbulence generated by a Smagorinsky-type LES, J. Fluid Mech. 325 (1996) 239–260.
[13] P.J. Mason, Large-eddy simulation: a critical review of the technique, Q. J. R. Meteorol. Soc. 120 (1994) 1–26.
[14] D.C. Leslie, G.L. Quarini, The application of turbulence theory to the formulation of subgrid modelling procedures, J. Fluid Mech. 91 (1979) 65–91.
[15] P.J. Mason, D.J. Thomson, Stochastic backscatter in large-eddy simulations of boundary layers, J. Fluid Mech. 242 (1992) 51–78.
[16] B. Kosović, Subgrid-scale modelling for the large-eddy simulation of high-Reynolds-number boundary layers, J. Fluid Mech. 336 (1997) 151–182.
[17] C.E. Leith, Stochastic backscatter in a subgrid-scale model: plane shear mixing layer, Phys. Fluids 2 (1990) 297–299.
[18] U. Schumann, Stochastic backscatter of turbulence energy and scalar variance by random subgrid-scale fluxes, Proc. Roy. Soc. London Ser. A. 451 (1995) 293–318.

[19] C. Hărtel, F. Kleiser, Analysis and modelling of subgrid-scale motions in the near-wall turbulence, J. Fluid Mech. 356 (1998) 327–352.
[20] D.C. Dunn, J.F. Morrison, Analysis of coherent structures in turbulent channel flow using the orthogonal wavelet representation, in: C. Dopazo (Ed.), Advances in Turbulence VIII, CIMNE, Barcelona, 2000, pp. 671–674.
[21] D.C. Dunn, J.F. Morrison, Effects of anisotropy on energy transfer in near-wall turbulence, in: I.P. Castro, P.E. Hancock (Eds.), Advances in Turbulence IX, CIMNE, Barcelona, 2002, pp. 599–603.
[22] D.C. Dunn, J.F. Morrison, Anisotropy and energy flux in wall turbulence, J. Fluid Mech. 491 (2003) 353–378.
[23] D.C. Dunn, J.F. Morrison, Analysis of the energy budget in turbulent channel flow using orthogonal wavelets, Computers and Fluids (2004), in press.
[24] R. Akhavan, A. Ansari, S. Kang, N. Mangiavacchi, Subgrid-scale interactions in a numerically simulated planar jet and implications for modelling, J. Fluid Mech. 408 (2000) 83–120.
[25] D. Carati, S. Ghosal, P. Moin, On the representation of backscatter in dynamic localization models, Phys. Fluids 7 (2000) 606–616.
[26] J.A. Murray, U. Piomelli, J.M. Wallace, Spatial and temporal filtering of experimental data for a priori studies of subgrid-scale stresses, Phys. Fluids 8 (1996) 1978–1980.
[27] S. Liu, C. Meneveau, J. Katz, On the properties of similarity subgrid-scale models as deduced from measurements in a turbulent jet, J. Fluid Mech. 275 (1994) 83–119.
[28] C. Meneveau, Statistics of turbulence subgrid-scale stresses: necessary conditions and experimental tests, Phys. Fluids 6 (1994) 815–833.
[29] U. Piomelli, E. Balaras, Wall-layer models for large-eddy simulations, Ann. Rev. Fluid Mech. 34 (1994) 349–374.
[30] S.K. Robinson, An experimental search for near-wall boundary conditions for LES, 1982, AIAA-82-0963.
[31] J.R. Chasnov, Simulation of the kolmogorov intertial subrange using an improved subgrid model, Phys. Fluids 3 (1991) 188–200.
[32] N.D. Sandham, R.J.A. Howard, Statistics databases from direct numerical simulation of fully-developed turbulent channel flow, Technical Report Report No. QMW-EP-1106, Queen Mary and Westfield College, University of London, 1995.
[33] P. Bradshaw, Conditions for the existence of an inertial subrange in turbulent flow, Technical Report Aero. Rep. No. 1220, Natl. Phys. Lab., 1967.
[34] S.G. Saddoughi, S.V. Veeravalli, Local isotropy in turbulent boundary layers at high reynolds number, J. Fluid Mech. 268 (1994) 333–372.
[35] P. Mestayer, Local anisotropy in a high-Reynolds-number turbulent boundary layer, J. Fluid Mech. 125 (1982) 475–503.
[36] T.S. Lund, On the use of discrete filters for large eddy simulations, Technical Report Center for Turbulence Research Annual Research Briefs, Stanford University, 1997.
[37] C. Hărtel, L. Kleiser, Galilean invariance and filtering dependence of near-wall grid-scale/subgrid-scale interactions in large-eddy simulation, Phys. Fluids 9 (1997) 473–475.
[38] I. Marusic, G.J. Kunkel, F. Porté-Agel, Experimental study of wall boundary conditions for large eddy simulations, J. Fluid Mech. 446 (2001) 309–320.
[39] J.F. Morrison, B.J. McKeon, W. Jiang, A.J. Smits, Scaling of the streamwise velocity component in turbulent pipe flow, J. Fluid Mech. (2004), in press.